Pacific Northwest
NATIONAL LABORATORY

PNNL-28619

Stage B Uranium Sequestration Amendment Delivery Monitoring Using Time-Lapse Electrical Resistivity Tomography

April 2019

TC Johnson
JN Thomle
JL Robinson
RD Mackley
MJ Truex

U.S. DEPARTMENT OF ENERGY

Prepared for the U.S. Department of Energy
under Contract DE-AC05-76RL01830

PACIFIC NORTHWEST NATIONAL LABORATORY
operated by
BATTELLE
for the
UNITED STATES DEPARTMENT OF ENERGY
under Contract DE-AC05-76RL01830

Printed in the United States of America

Available to DOE and DOE contractors from the
Office of Scientific and Technical Information,
P.O. Box 62, Oak Ridge, TN 37831-0062;
ph: (865) 576-8401
fax: (865) 576-5728
email: reports@adonis.osti.gov

Available to the public from the National Technical Information Service
5301 Shawnee Rd., Alexandria, VA 22312
ph: (800) 553-NTIS (6847)
email: orders@ntis.gov <https://www.ntis.gov/about>
Online ordering: http://www.ntis.gov

PNNL-28619

Stage B Uranium Sequestration Amendment Delivery Monitoring Using Time-Lapse Electrical Resistivity Tomography

April 2019

TC Johnson
JN Thomle
JL Robinson
RD Mackley
MJ Truex

Prepared for
the U.S. Department of Energy
under Contract DE-AC05-76RL01830

Pacific Northwest National Laboratory
Richland, Washington 99354

Summary

The Hanford Site 300 Area lies adjacent to the Columbia River, approximately 5 km north of Richland, Washington. Past waste disposal practices in the 300 Area resulted in vadose zone uranium contamination beneath former infiltration ponds and trenches. Stage-driven water table fluctuations and river water intrusion facilitate mobilization of uranium from contaminated sediments in regions periodically occupied by the water table (i.e., the periodically rewetted zone or PRZ), thereby raising groundwater uranium concentrations above the maximum allowable contaminant level for uranium.

Enhanced attenuation of uranium using phosphate treatment was selected as part of the remedy in the 300 Area Record of Decision (EPA and DOE, 2013). From September 4-20, 2018, in accordance with DOE/RL-2014-42-ADD1, CH2M Hill Plateau Remediation Company conducted an in situ uranium sequestration remedy by injecting a phosphate amendment through injection wells installed in a select region of the 300 Area PRZ and the lower vadose zone (LVZ), which is the region of the vadose zone directly above the PRZ. Real-time cross-borehole electrical resistivity tomography (ERT) was used to evaluate amendment delivery by imaging the spatial and temporal distribution of the change in subsurface electrical conductivity caused by amendment migration. ERT imaging surveys were conducted continuously using wellbore annulus electrodes installed in three clusters of injection and monitoring boreholes. On each cluster, surveys were conducted every 52 minutes and images were reported via website in near-real time.

This report documents the ERT imaging operations and interpretation of imaging results in terms of the extent of amendment delivery (including phosphate and/or carrier fluid) within the treatment area. Based on the interpretation, amendment delivery to the LVZ and PRZ was observed to be variable between each of the three imaging clusters, as shown in Figure S.1. Amendment transport in Cluster 1 exhibited significant lateral flow in comparison to Clusters 2 and 3, resulting in a final amendment distribution throughout a large portion of the LVZ and PRZ sediment between the injection wells. Cluster 2 exhibited good amendment delivery in the LVZ only near the injection wells. In the PRZ at Cluster 2, amendment was effectively distributed through the full distance between injection wells. Cluster 3 exhibited the smallest amount of lateral flow and amendment was primarily distributed in the LVZ and PRZ very near the injection wells. Imaging results below the water table suggest that more amendment entered the groundwater in Cluster 2 and Cluster 3 than in Cluster 1.

Lateral transport within the three clusters is correlated with differences in bulk electrical conductivity between LVZ and PRZ sediments evident in baseline static ERT imaging. Each cluster exhibited relatively layered bulk conductivity structure within the LVZ and PRZ, which is consistent with layers of finer and coarser materials that tend to exhibit higher and lower levels of saturation respectively. Each cluster also exhibited lateral variations in bulk conductivity, which are diagnostic of changes in sediment properties or states (such as sediment texture, porosity, saturation, and pore fluid conductivity). Cluster 1 exhibited markedly higher baseline bulk electrical conductivity structure than Cluster 2 or Cluster 3, which may have been caused by horizontally continuous, relatively fine-grained zones of sediment, or alternating layers of coarse and fine textured sediments that promote lateral transport. Overall, amendment coverage variability within the LVZ and PRZ appears to have resulted primarily from variability in hydrogeologic properties that may have been influence in part by legacy waste discharge operations and past remediation excavations.

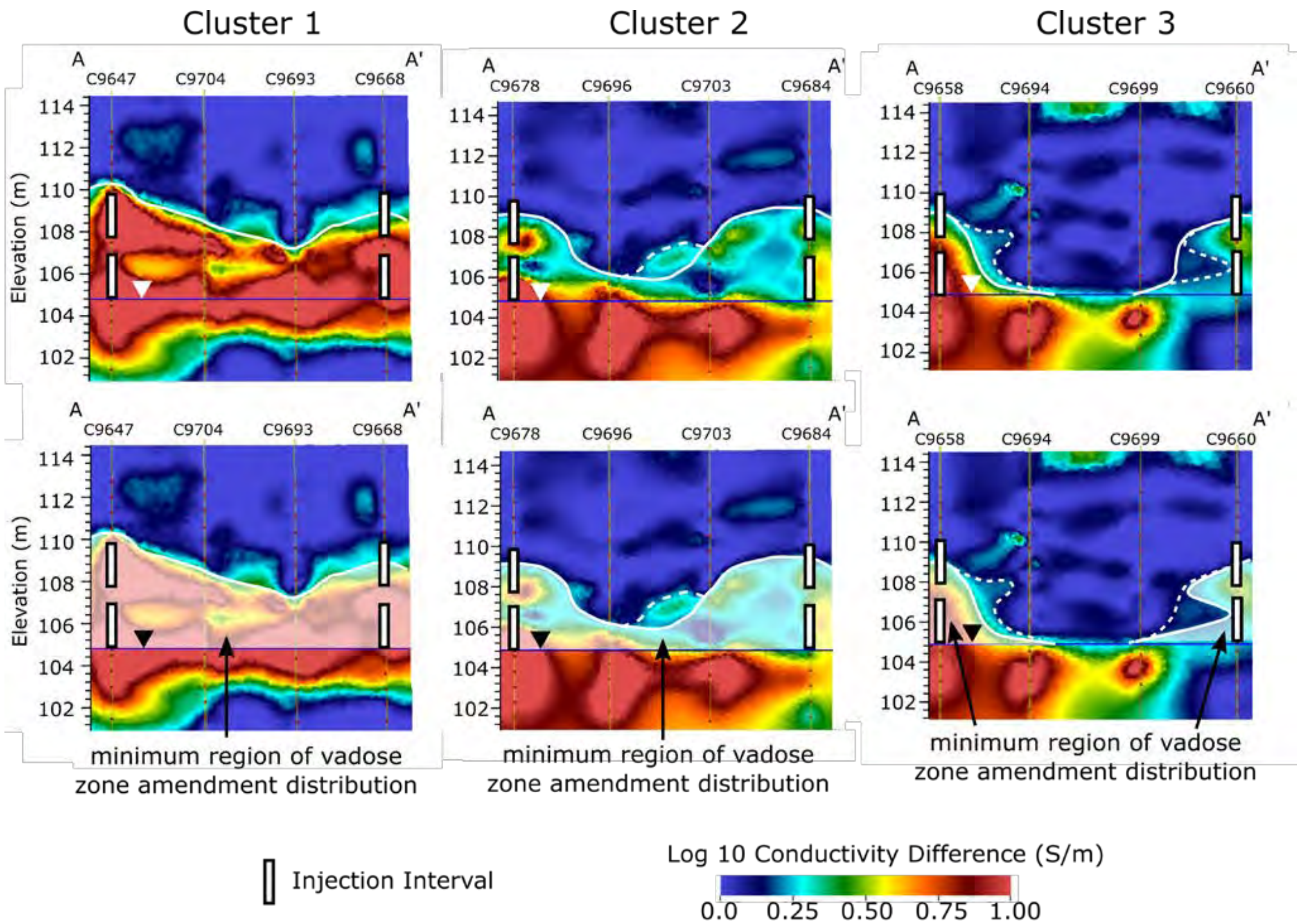

Figure S.1. Summary images showing the largest changes in bulk conductivity during amendment injections for each of the three clusters. The top row shows maximum increase in conductivity observed over the monitoring period. The bottom row shows the corresponding interpretation of the amendment-distribution zone above the water table shaded in white and bounded by white lines. Dashed lines show alternate interpretations of amendment-distribution zone.

Acknowledgments

This work was funded by the CH2M Hill Plateau Remediation Company under contract 49517-49 in support of the 300-FF-5 Operable Unit Stage B Uranium Sequestration test. We would like to recognize the technical collaboration and review provided by the 300-FF-5 Stage B Project team members Dave St. John (CHPRC), Sarah Springer (CHPRC), Sunil Mehta (INTERA), Elyse Frohling, (CHPRC), Virginia Rohay (CHPRC), and Ryan Nell (INTERA).

Acronyms and Abbreviations

ERT	electrical resistivity tomography
LVZ	lower vadose zone
PNNL	Pacific Northwest National Laboratory
PRZ	periodically rewetted zone

Nomenclature

$\sigma_{b,t}$	bulk electrical conductivity at time *t*
θ	porosity
m	Archie's cementation exponent
n	Archie's saturation exponent
$\sigma_{f,t}$	pore water fluid electrical conductivity at time *t*
S_t	saturation at time *t*
$\sigma_{s,t}$	pore/grain interface electrical conductivity at time *t*
$S_{pw,t}$	fraction of saturation attributed to pore water at time *t*
$S_{p,t}$	fraction of saturation attributed to phosphate amendment at time *t*
σ_{pw}	pore water conductivity
σ_p	phosphate amendment conductivity

Contents

Figures

Tables

1.0 Introduction

1.1 Site Overview and Background

The Hanford Site is located in Washington State, north of the city of Richland. From 1942 to 1988, the primary mission of the Hanford Site was weapons-grade plutonium production. During production operations, waste disposal practices left many areas with vadose zone and groundwater contamination (Figure 1). The 300 Area was the primary research center and housed fabrication facilities for the uranium fuel rods used in the plutonium production process. Between 1943 and 1975, liquid waste from research and fabrication operations in the 300 Area was disposed in process ponds (north and south). Additional waste from the 300 Area operations was discharged to the subsurface between 1975 and 1985. Much of the sediment contained in the 300 Area process ponds was excavated in the mid-1990s and replaced with clean fill in 2004 (DOE-RL-2005-41 2005; Williams et al. 2007). However, uranium contamination persisted deeper in the vadose zone and is now the primary contamination of concern. The 2017 uranium plume in the 300 Area is shown in Figure 2. Leaching of uranium from contaminated sediments in the lower vadose zone (LVZ) and periodically rewetted zone (PRZ) to the aquifer is largely driven by Columbia River stage levels. At higher river stages, the water table rises further into the PRZ and mobilizes uranium from contaminated sediment (depicted in Figure 3) and elevates the aqueous uranium concentrations above the cleanup level of 30 μg/L (the resulting uranium plume shown in Figure 2).

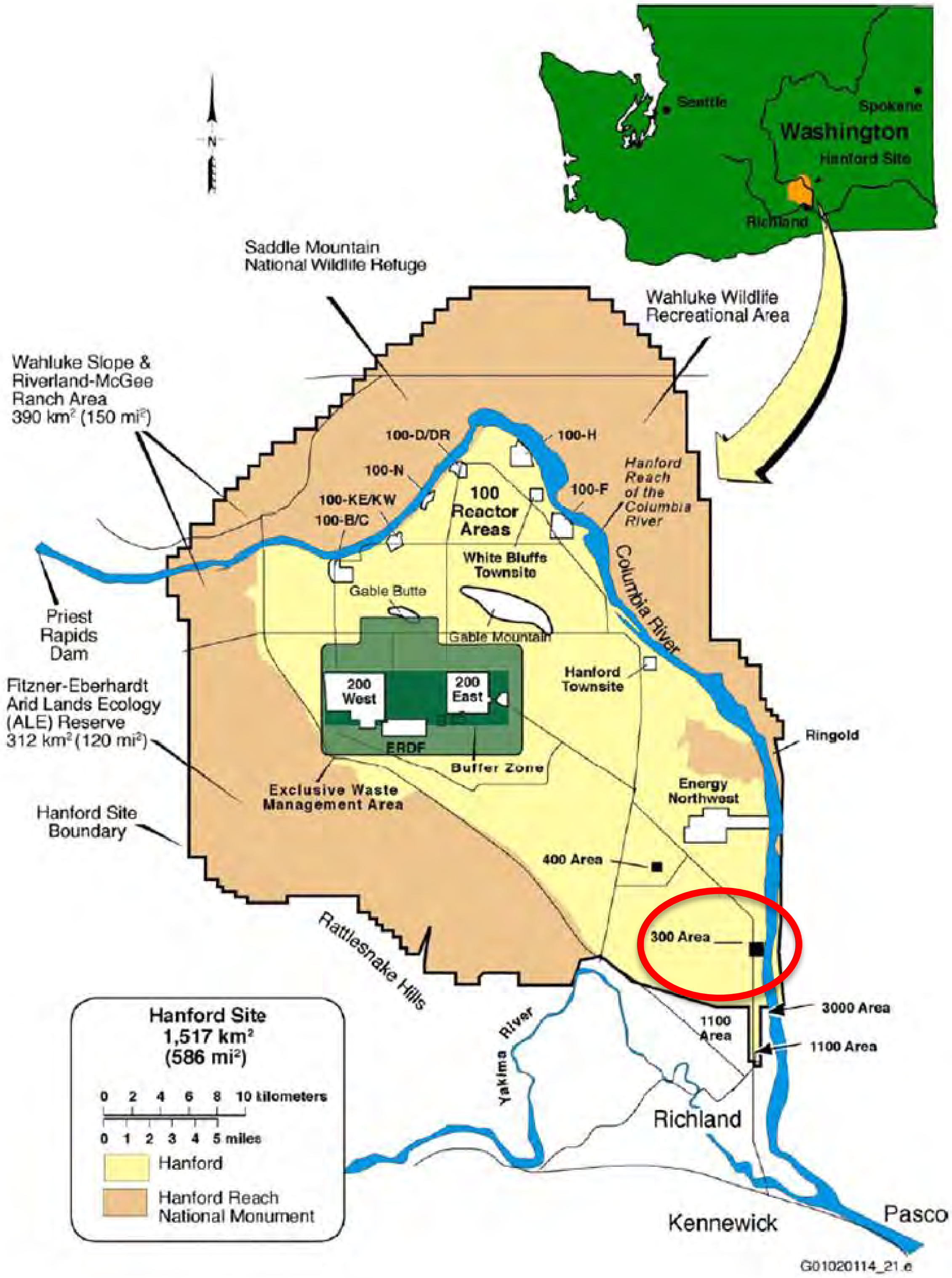

Figure 1. The 300 Area is located in the southeast corner of the Hanford Site, north of Richland, Washington (Peterson et al. 2008).

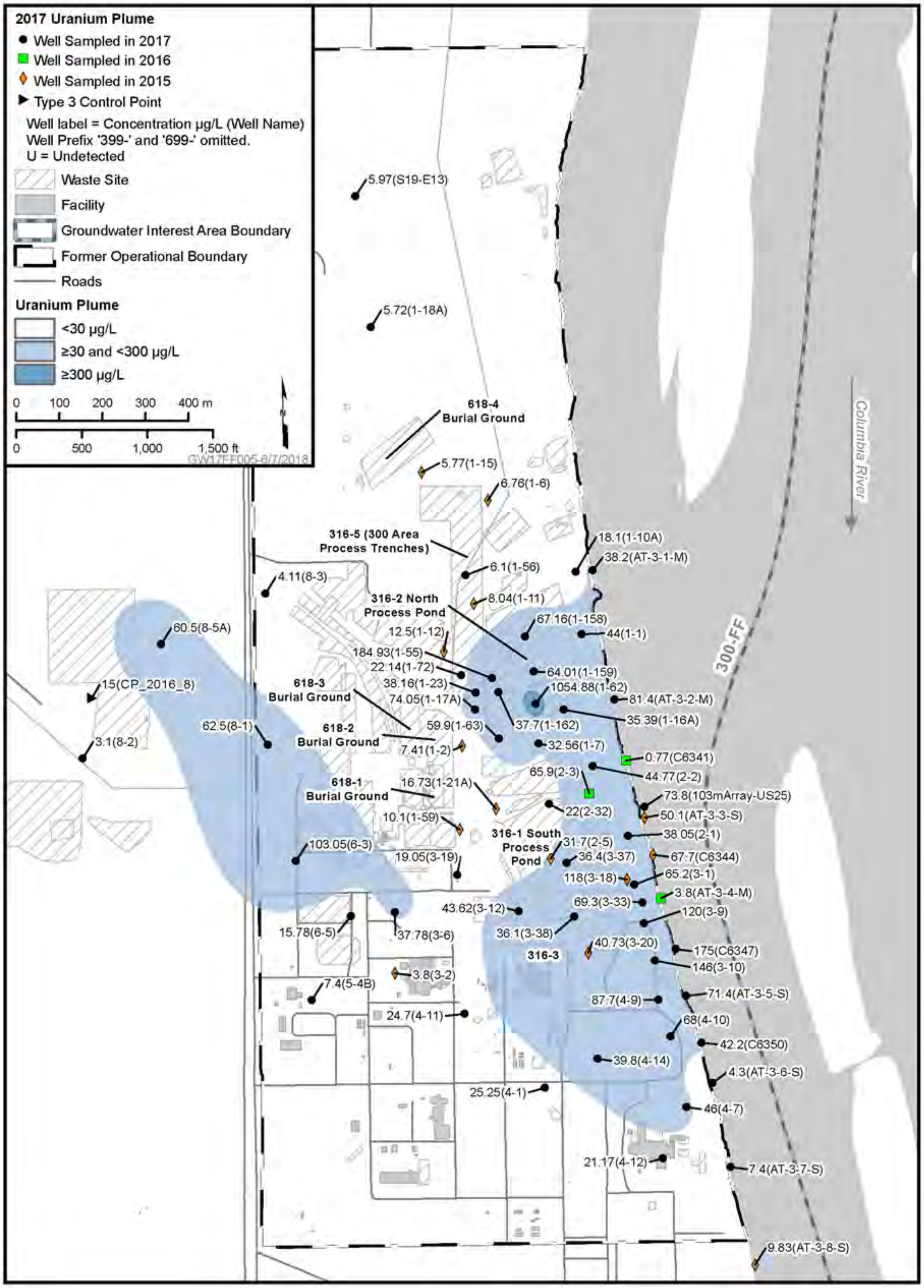

Figure 2. 2017 Uranium Groundwater Plume in the 300 Area (DOE_RL-2017-66 Rev 0).

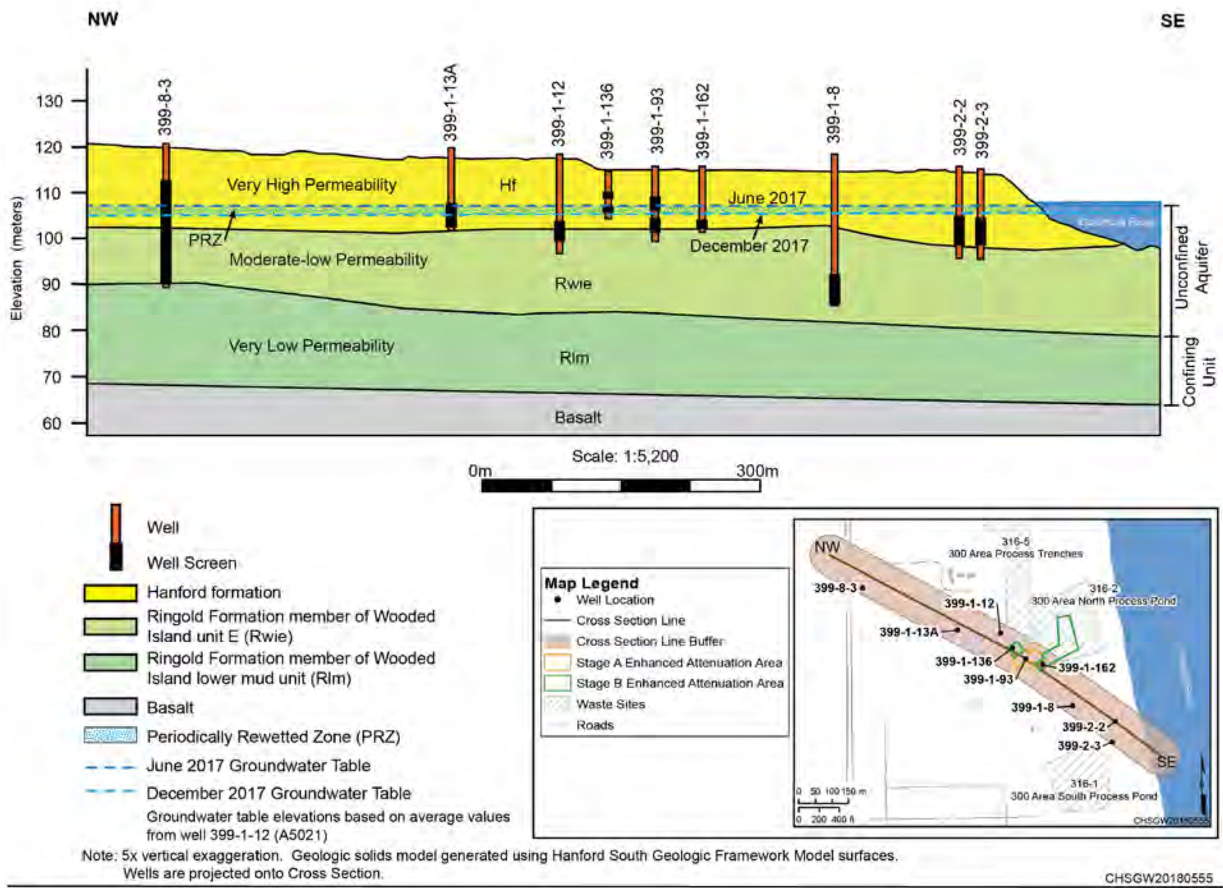

Figure 3. Cross-Section Showing the Relation between the Water Table, PRZ, and River Stage in the 300 Area (SGW-60778 Rev 0).

In an effort to immobilize uranium contamination in the vadose zone and PRZ, a treatment method was developed using phosphate, which has been shown to reduce uranium mobility by forming uranium phosphate precipitates and coating surface phases of uranium with stable mineral phases (Szecsody et al. 2012). Enhanced attenuation of uranium using phosphate treatment was selected as part of the remedy in the 300 Area Record of Decision (EPA and DOE, 2013). From September 4-20, 2018, in accordance with DOE/RL-2014-42-ADD1, CH2M Hill Plateau Remediation Company treated a 0.9 ha (2.25 acre) area within the Stage B Enhanced Attenuation Area in the 300 Area (Figure 4), which was thought to contain the highest mobile uranium concentrations. The phosphate amendment included a solution of monosodium phosphate and pyrophosphate that was injected directly into the LVZ and PRZ.

Electrical resistivity tomography (ERT), a geophysical imaging method, was used as one of the methods for monitoring phosphate amendment migration and assessing performance of the amendment delivery system. Static ERT images spatial changes in bulk electrical conductivity caused by variations in porosity, saturation, and pore fluid electrical conductivity, thereby providing information on both the physical and chemical state of the imaging zone. Time-lapse ERT images temporal changes in the bulk electrical conductivity, which are caused (in this case) by changes in saturation and pore fluid conductivity during polyphosphate amendment injections. ERT uses an array of electrodes to induce electrical current flow within the subsurface and to measure the resulting electrical potential. These measurements are then processed using a tomographic algorithm to recover, or image, the subsurface electrical conductivity distribution that gave rise to the measurements (Johnson et al. 2010). Using electrode arrays installed on selected injection and monitoring wellbore casings (i.e., within the wellbore annulus) changes in electrical conductivity induced by phosphate amendment were monitored in a 2D cross section between selected injection wells for the duration of treatment operations to help assess amendment delivery, migration, and overall coverage within the vadose zone and shallow groundwater. This report describes the petrophysical underpinnings that connect changes in bulk electrical conductivity to amendment-induced changes in pore fluid conductivity and saturation, the layout of the ERT system within the treatment area, ERT operations, ERT imaging results during monitoring, and the interpretation of the resulting data.

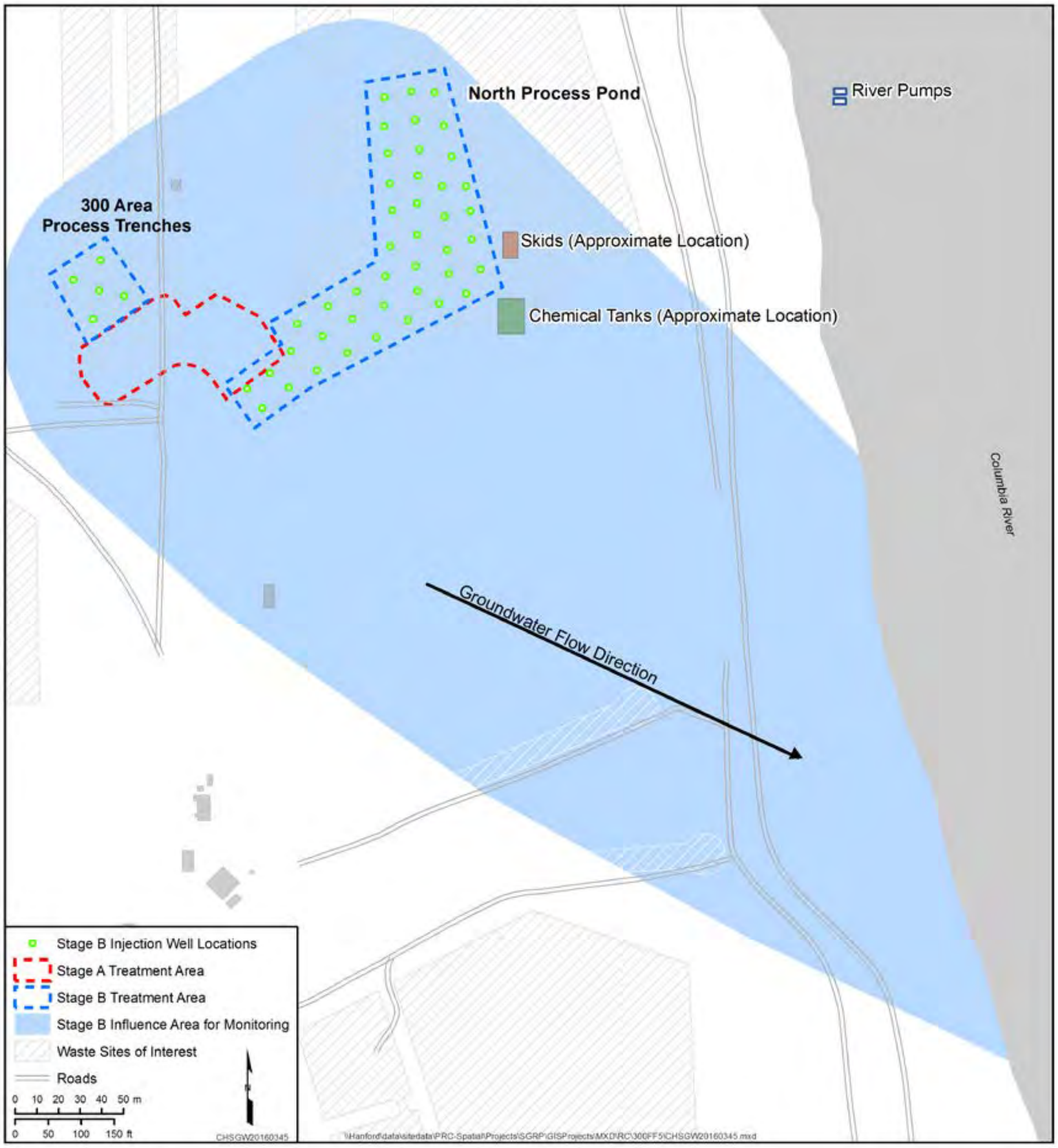

Figure 4. Stage B Enhanced Attenuation Area General Site Layout (DOE/RL-2014-42-ADD1 Rev 0).

1.2 ERT Imaging, Petrophysics, and Image Interpretation

1.2.1 Overview

The objective of ERT is to estimate the bulk electrical conductivity distribution of the subsurface through tomographic imaging. A single ERT measurement is collected by injecting current between a pair of electrodes and measuring the resulting voltage across several other electrode pairs. Using an array of electrodes, many such measurements are strategically collected to optimize resolution of the bulk conductivity image. This set of measurements, termed herein an ERT survey, is processed using a computationally intensive tomographic inversion algorithm that approximates the subsurface conductivity distribution that gave rise to the measurements (Johnson et al. 2010). When time-lapse imaging is conducted, surveys are continuously collected and processed to provide a chronological sequence of image frames that illustrate the change in bulk conductivity with time. Subtracting the baseline image (i.e., the pretreatment image in this case) from the time-lapse images reveals the change in bulk conductivity caused by the phosphate amendment, thereby revealing the distribution of amendment in space and time. The time-lapse images may then be analyzed to investigate amendment delivery performance and timing, subject to the resolution limitations of ERT imaging as described below.

1.2.2 Relationships between Amendment Concentration, Soil Properties, and Bulk Electrical Conductivity

The bulk electrical conductivity of porous media is governed by porosity, saturation, pore fluid electrical conductivity, mineral surface conductivity, and pore-space tortuosity as described by Slater and Lesmes (2002):

$$\sigma_{b,t} = \theta^m \sigma_{f,t} S_t^n + \sigma_{s,t} \quad (1.1)$$

where $\sigma_{b,t}$ is the bulk electrical conductivity at time t, θ is porosity, $\sigma_{f,t}$ is the pore fluid conductivity at time t, S_t^n is the saturation at time t, and $\sigma_{s,t}$ is the surface conductivity at time t, which accounts for conduction along the pore-grain interface. For unconsolidated sediments, the cementation factor m is typically 1.35 to 1.6 and the saturation exponent n is typically near 2.0 for 300 Area vadose zone sediments (Johnson et al. 2010). Introduction of phosphate amendment into the subsurface increases both saturation and pore fluid electrical conductivity (due to the high ionic strength of the amendment), thereby increasing bulk conductivity and providing a target for time-lapse ERT imaging. Assuming that the change in $\sigma_{s,t}$ with time is insignificant, the change in bulk conductivity caused by the phosphate amendment from some baseline condition at time 0 to time t can be expressed as:

$$\Delta\sigma_{b,t} = \theta^m (\sigma_{f,t} S_t^n - \sigma_{f,0} S_0^n) \quad (1.2)$$

Note here that the bulk conductivity distribution at time t, $\Delta\sigma_{b,t}$, is estimated through time-lapse ERT imaging. In particular, the phosphate amendment injections are expected to increase pore fluid conductivity (σ_f) below the water table and to increase both σ_f and saturation (S) above the water table. Eq. 1.2 demonstrates that although the increase in pore fluid conductivity and saturation produced by the introduction of amendment causes a corresponding increase in bulk conductivity, the change in bulk conductivity alone cannot be used to uniquely determine pore fluid conductivity (and thus amendment concentration) or saturation at a given time. Consequently, ERT cannot identify whether amendment transport is conservative, or equivalently whether the polyphosphate is being transported with the carrier fluid. However, time-lapse changes in bulk conductivity provided by ERT can be used to estimate the distribution of amendment solution (polyphosphate and/or carrier fluid) with time, thereby providing important information concerning the overall performance and timing of amendment delivery.

1.2.3 Image Interpretation in the Context of Limited Resolution

Valid assessment of time-lapse ERT images requires adequate accounting for the effects of limited imaging resolution. ERT data do not provide enough information to uniquely estimate the distribution of subsurface bulk conductivity. This problem is addressed by constraining the ERT imaging algorithm to provide only the spatial heterogeneity that is required to fit the survey data. Consequently, ERT images are a smoothed, spatially averaged representation of the true subsurface bulk conductivity. Image smoothing increases or resolution decreases with distance from ERT electrodes.

The effects of limited resolution could be equivalently described in terms of the ERT sampling volume. That is, the bulk conductivity of a given point in the ERT image is a weighted average of the true bulk conductivity over some volume surrounding that point. The size of that volume increases with distance from the electrodes. This concept is shown schematically in Figure 5.

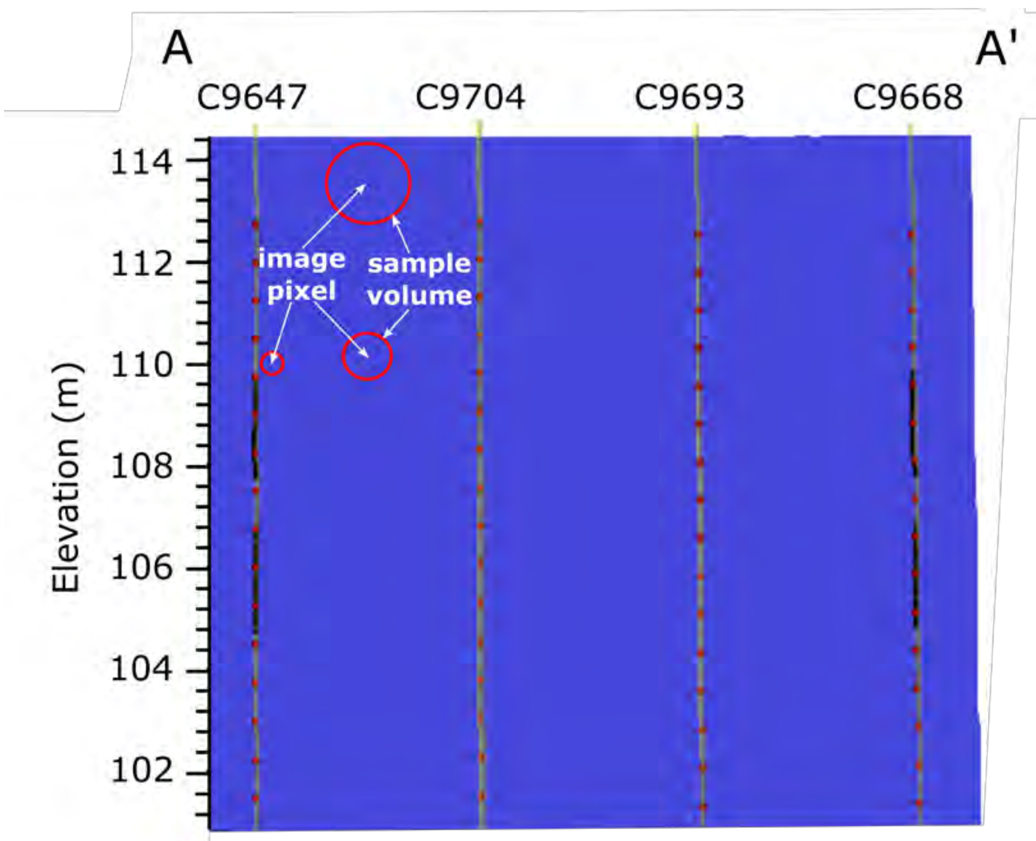

Figure 5. Conceptual diagram illustrating the effects of limited resolution. Each pixel in the ERT image is the weighted average of the true bulk conductivity over some sampling volume. The size of the sampling volume increases with distance from the electrodes, resulting in a loss of resolution with distance from instrumented wellbores.

The spatial averaging caused by limited resolution generally results in high values being underpredicted and low values being overpredicted in the ERT image, thereby making quantitative analysis of specific concentrations at a selected location based on ERT images unreliable. Because of this, all observations, calculations, interpretations, and general conclusions derived from the ERT images must be understood in the context of the image resolution. For this reason, interpretation of ERT results for relative changes over time is the most appropriate application. Thus, use for assessing spatial changes in bulk conductivity that correspond to amendment movement in the subsurface is appropriate, while use of the images to define amendment concentration is not.

ERT electrode and survey design were conducted prior to deployment to define an electrode array that would provide suitable resolution for the monitoring objective. For the 300 Area, this design resulted in a series of electrodes distributed in vertical arrays at the selected injection and monitoring wells. The resolution of this ERT system design was considered in providing images and their interpretation for use in evaluating amendment delivery.

2.0 Site Layout

2.1 Wellfield Layout and ERT Imaging Clusters

Figure 6 shows a plan view of the Stage B phosphate treatment area. The site consisted of 48 injection wells and 18 monitoring wells. Amendment injections were executed sequentially in four injection zones distributed evenly throughout the treatment area, as indicated by the yellow, green, blue, and pink areas respectively. The two injection skids provided sufficient volume for treatment of 12 wells simultaneously. Three groups of wells, Clusters 1-3, were instrumented with ERT electrodes to enable cross-hole ERT imaging. Each cluster included four bounding injection wells and two interior monitoring wells. Based on site characterization data, cluster locations were chosen to collectively provide imaging results representative of site variability and groundwater flow, and to straddle each of the injection zones. Straddling the injection zones enabled the time-lapse ERT imaging within a given cluster to independently assess the relative performance of the two injection zones traversed by that cluster.

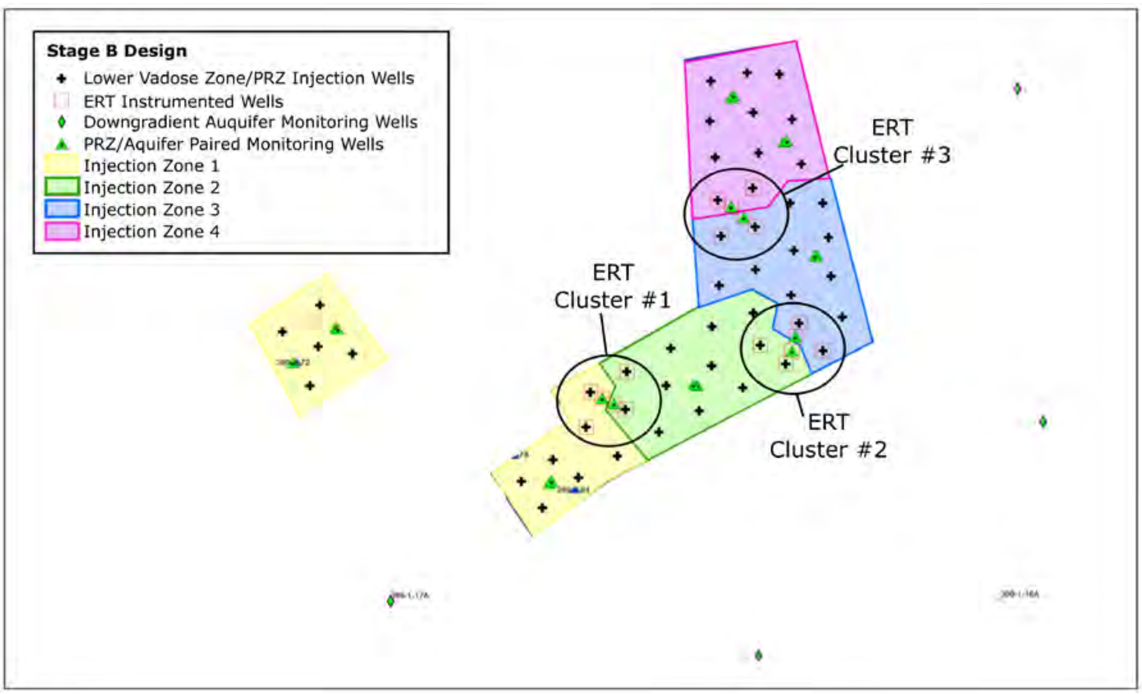

Figure 6. 300 Area Stage-B treatment area layout.

Figure 7 shows plan view details of each ERT monitoring well cluster (left column) and a diagram of the electrode distribution for each cluster (right column). Each ERT well was instrumented with 16 electrodes at 0.75 m spacing to span a vertical interval of 11.25 m. Although ERT data processing was conducted in three dimensions for each cluster, ERT images are shown only in the A-A’ and B-B’ planes in this report. Horizontal ERT wellbore offsets in the A-A’ planes range from 4.3 m to 5.5 m overall, which provides adequate resolution between wellbores, given the 11.25 m vertical electrode interval. Thus, results for the A-A’ plane is emphasized in the data analysis as the most useful to support interpretation of amendment delivery.

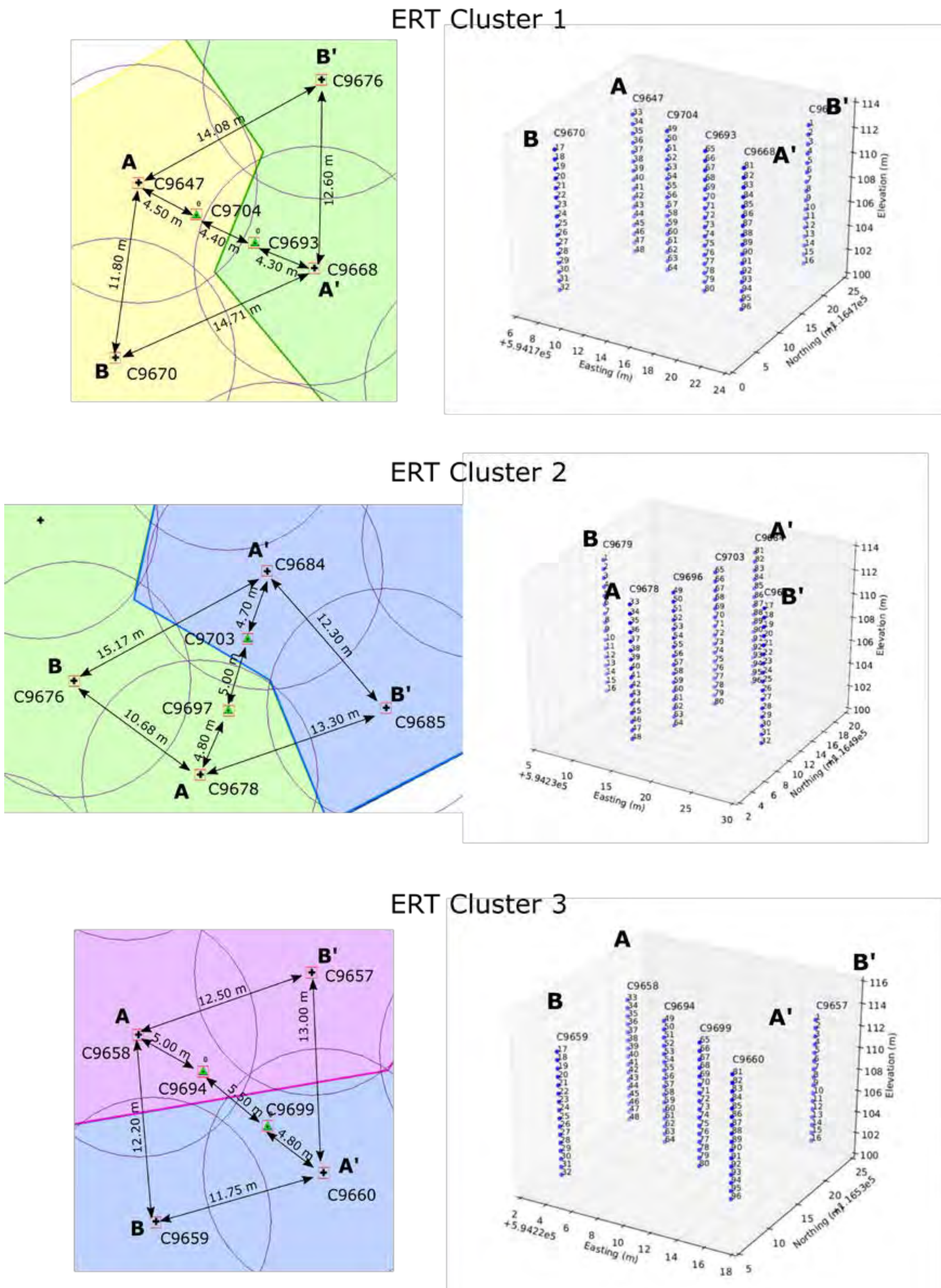

Figure 7. ERT cluster wellbore orientations (left column) and electrode positions (right column). Area coloring represents corresponding injection zone in Figure 6. Purple curves represent anticipate amendment coverage zone for each injection well (+ symbols). Each well in the cluster has 16 electrodes at 0.75 m spacing.

In the B-B' planes, horizontal wellbore offsets are too large to provide adequate resolution between wellbores. In those planes, imaging results should only be considered valid in the near wellbore regions and where the B-B' planes intersect the A-A' planes, as will be shown in the forthcoming results.

Figure 8 shows a diagram of the A-A' cross-section for Cluster 1, which is equivalent for Clusters 2 and 3 in the vertical dimension. Each outer well in the section is an injection well with two screened intervals; the PRZ intervals ranging from 105 m to 107 m in elevation and the LVZ intervals ranging from 108 m to 110 m in elevation. The PRZ intervals span the approximate vertical interval occupied by the water table during high and low river stage of a nominal year and were the target zone for amendment delivery.

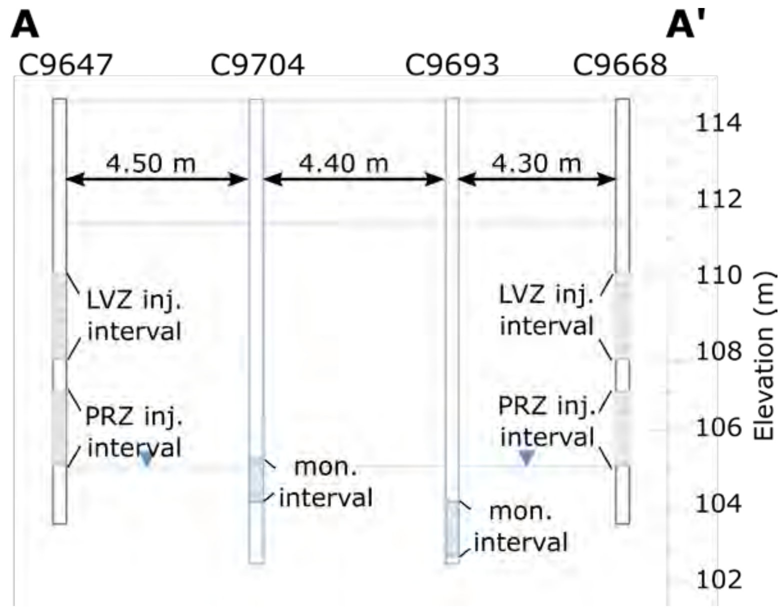

Figure 8. Cross-section for A-A' line in ERT Cluster 1. Screened interval elevations are equivalent in Clusters 2 and 3, with well separations as indicated in Figure 7.

2.2 Wellbore Electrode Arrays

Figure 9 shows the design detail for the electrode array installation on each ERT well. The uppermost electrode was installed 2.0 m below ground surface, with each subsequent electrode installed 0.75 m further down the casing for a total depth of 13.25 m to the bottom electrode. As shown in Figure 10, each electrode consisted of a 10 cm tall section of stainless-steel wire mesh attached to the outside of the polyvinyl chloride casing using two low-profile stainless-steel band clamps. Each electrode was then attached to a multiconductor ERT cable through a "takeout," or a stainless-steel cylinder internally attached to one of the conductors (i.e., wires) within the ERT cable. The ERT cables were waterproof with tensile strength of 300 lbs. and custom ordered through a commercial ERT cable fabrication company. Figure 11 shows a scaled drawing of an ERT cable takeout. The widest section of the takeout was the waterproof polyethylene takeout jacket, which had a diameter of 22 mm (7/8 inches). Ultimately, the maximum width of the electrode array was approximately 2.5 cm wider than the 10.2 cm (4 inch) diameter wellbore casing, forming a low-profile array for easy deployment within the borehole.

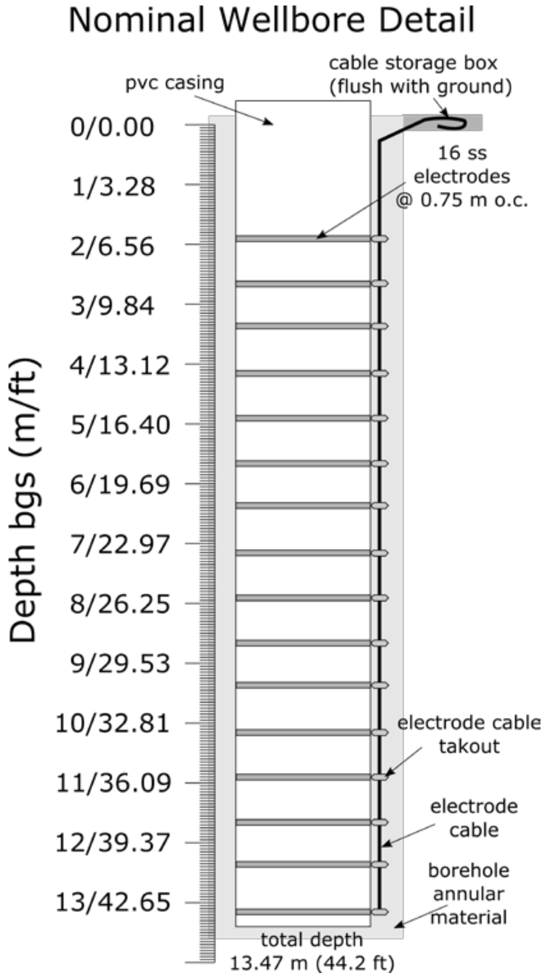

Figure 9. Nominal ERT wellbore construction detail (screened intervals are not shown).

Borehole electrode installation proceeded as follows:

1. Borehole was drilled and drill casing advanced to total depth.
2. Polyvinyl chloride casing or screened interval was advanced down the inside of the drill casing (nominally 10 ft threaded lengths). ERT electrodes and cable were attached to the casing as it was advanced downhole.
3. Electrode array/casing system was deployed to total depth, and drill casing was retracted.
4. Annular space was completed with engineered non-bentonite cement grout in solid intervals (Section 2.3) and with engineered sand in screened sections.
5. Wellbore pad was constructed, including surface-mount box for the ERT cable extension and cable head.

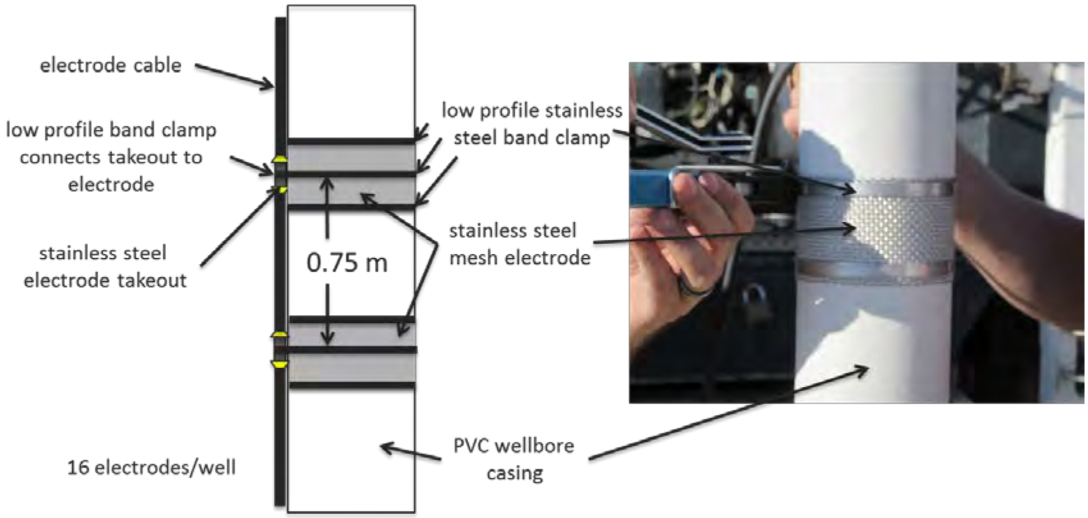

Figure 10. Diagram of electrode and electrode cable installation on wellbore casing (left) and corresponding photograph (right).

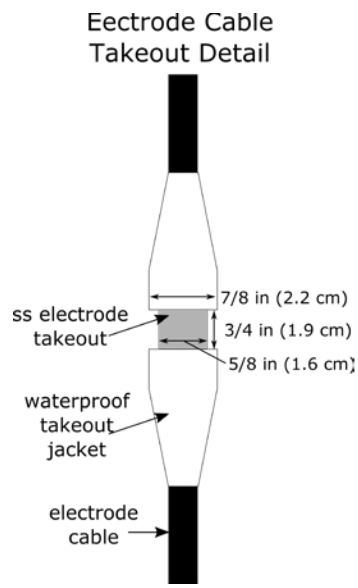

Figure 11. Drawing of ERT cable takeout.

2.3 Wellbore Annular Grout

Standard wellbore grouting materials (e.g., Portland cement) typically have cured electrical conductivities that are well above the native bulk electrical conductivity of saturated or unsaturated sands and gravels. These materials create preferred flow paths for electrical current during ERT imaging, which reduces sensitivity to the formation and causes wellbore artifacts in the ERT images. Ideally, wellbore grouting materials should have lower conductivity than native formation materials, which encourages current flow through the formation, thereby increasing sensitivity to the formation and improving imaging resolution. To achieve this objective, the unscreened portions of each wellbore were finished with an annular grout engineered for ERT applications to have low conductivity. The grout cement consisted of one part Type I Portland Cement to three parts DS-325 Hess Pozzalon at a 0.54 water/cement ratio. According to laboratory testing results, the annular grout should have achieved a conductivity of less than 3.5e-4 S/m after one year of curing, which exceeds the time from wellbore installation to baseline ERT imaging. Minimum formation conductivities estimated from baseline ERT imaging were approximately 5.0e-4 S/m (see Section 4.1), suggesting that grout conductivity was less than formation conductivity within the ERT imaging zone.

3.0 ERT Operations

3.1 Phosphate Treatment Schedule

The nominal phosphate treatment schedule as executed during field operations is shown in Table 1. Daily injections were executed by zone, in either the LVZ or PRZ screened intervals, except for September 11 and 16, 2018, when injections were switched for LVZ to PRZ intervals. Nominal injection flowrates ranged from 45-50 gpm of in each well of the active zone. End times represent the last flow rate recorded for a given day. Actual end time may be later than shown in Table 1.

Table 1. Phosphate Treatment Schedule

Date	Injection Zone	Injection Interval	Nominal Start Time	Nominal End Time
9/4/2018	1	PRZ	9:30 AM	3:20 PM +
9/5/2018	1	PRZ	8:15 AM	3:15 PM +
9/6/2018	1	PRZ	6:30 AM	2:30 PM +
9/7/2018	1	LVZ	8:00 AM	3:00 PM +
9/8/2018	1	LVZ	7:00 AM	2:45 PM +
9/9/2018	2	PRZ	7:20 AM	3:20 PM +
9/10/2018	2	PRZ	7:30 AM	3:30 PM +
9/11/2018	2	LVZ + PRZ	6:30 AM	3:30 PM +
9/12/2018	2	LVZ	7:30 AM	3:30 PM +
9/13/2018	3	PRZ	7:30 AM	4:00 PM +
9/14/2018	3	PRZ	6:30 AM	3:30 PM +
9/15/2018	3	LVZ+PRZ	6:30 AM	3:45 PM +
9/16/2018	3	LVZ + PRZ	7:20 AM	2:50 PM +
9/17/2018	4	PRZ	7:10 AM	3:30 PM +
9/18/2018	4	PRZ	6:50 AM	1:50 PM +
9/19/2018	4	LVZ	6:30 AM	3:30 PM +
9/20/2018	4	LVZ	6:45 AM	11:45 AM +

3.2 ERT Data Collection Schedule

Electrodes from each of the three clusters were simultaneously attached to a single ERT data acquisition system, which enabled all injections to be simultaneously monitored without reconfiguring the system. The data collection schedule was chosen to balance the tradeoff between adequate spatial and temporal imaging resolution. Using a four-electrode measurement (two current electrodes and two potential electrodes), there are $N(N-1)(N-2)(N-3)/8$ unique measurements that may be collected during a given survey, where N is the number of electrodes (288 in this case). Collecting all unique measurements is impractical because doing so would require an excessive amount of time between time-lapse images. For each cluster, a subset of measurements was chosen, based on E4D design assessment, that provided adequate imaging resolution and could be collected fast enough to capture phosphate migration during treatment. The same survey was collected on each cluster, each consisting of 1,442 in-well and cross-well dipole-dipole measurements. An eight-channel Multiphase Technologies (MPT) DAS-1 (http://www.mpt3d.com/das1.html) electrical impedance tomography control unit and four multiplexors (Figure 12) were used to collect the data. Each control unit and multiplexor accommodated 64 electrodes, with 16 electrodes (one ERT well) per cable. By optimizing the survey to use all eight channels (i.e., eight electrical potential measurements were collected per current injection) during every current measurement, each survey required approximately 12 minutes to complete, or 36 minutes for all three clusters to complete a survey. Accordingly, one ERT image was produced every 36 minutes on each cluster. Monitoring began August 30, 2018, and ran continuously until October 26, 2018, with four interruptions lasting between 1 and 4 hours due to power outages during generator maintenance.

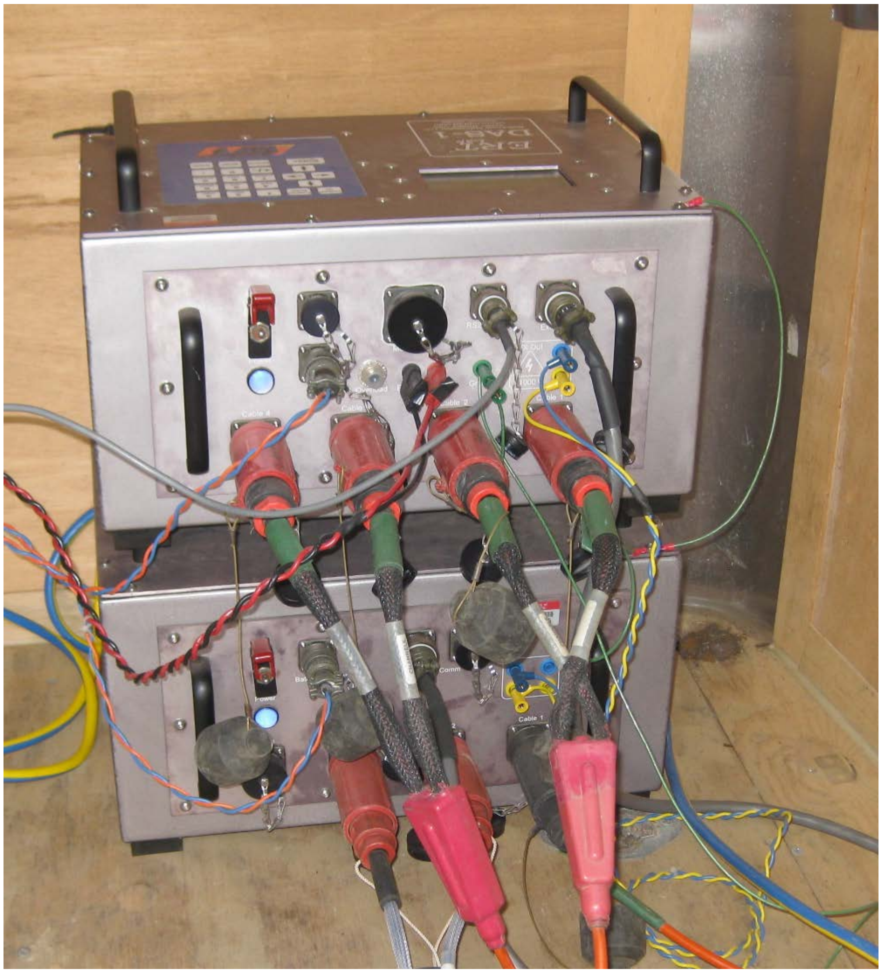

Figure 12. Example of DAS-1 electrical impedance tomography control on (top) with a single multiplexor (bottom).

3.3 ERT Data Processing

ERT data processing was automated from data collection through database archiving and presentation on a secure website, with the exception of one remote data transfer step. A flow diagram of the processing sequence is shown in Figure 13. In the first step, time-lapse surveys were continuously collected on the field data collection system, as described in the previous section. As each survey was completed, that survey was filtered for quality, reformatted, and submitted to a parallel computing system for processing via secured wireless internet connection. This step was completed by the field laptop computer connected to the data collection system. After processing, each time-lapse survey was archived in a database, and each image was submitted to a webserver for visualization on a password-protected website. This enabled site operators to visualize amendment distribution in near-real time during the treatment operation. The processing time required from the completion of a survey to submission of the ERT image to website was approximately 3-8 minutes, depending on the magnitude of the change in the data from the previous image. The maximum time required for website presentation was governed by the website refresh rate, which ranged from 15-30 minutes.

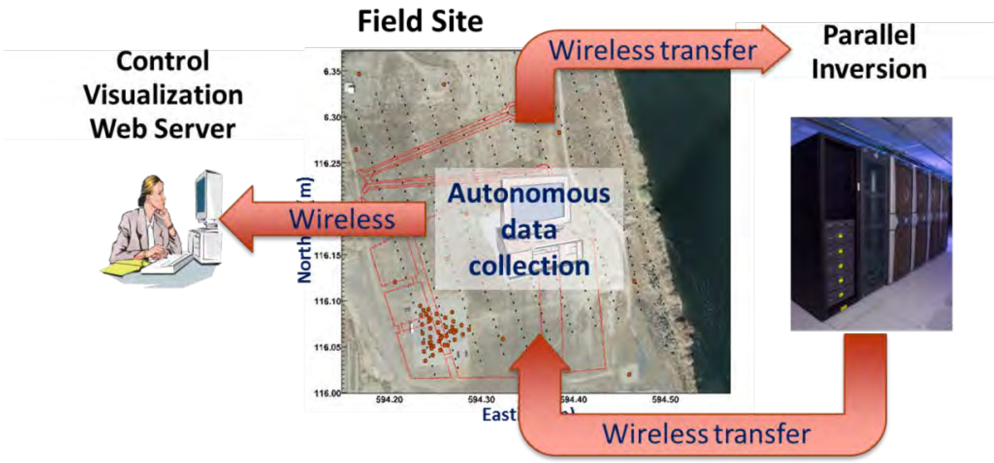

Figure 13. Autonomous ERT data control and processing flow diagram.

Rapid turnaround times were facilitated by using dedicated resources on the Pacific Northwest National Laboratory (PNNL) parallel computing system for the duration of the experiment. All processing was executed using E4D, a high-performance ERT imaging code developed at PNNL (https://e4d.pnnl.gov). E4D has been classified as safety software by PNNL and is NQA-1 level B qualified for software safety.

3.4 Website

To facilitate near-real-time delivery of the ERT images, results were delivered to a password-protected website. The website enabled users to animate the time-lapse images from the start of injections in a given zone to the current time to view the estimated distribution of amendment and the migration of amendment with time. A screenshot of the website showing the Cluster 1 A-A’ cross-section at 2:52 p.m. on September 5, 2018, during injection into the PRZ screen in well C6947 is shown in Figure 14. Users could optionally select which cluster and cross-section to view, step through the imaging sequence to the current time, and download the image frame for a given time step. This website tool is part of the SOCRATES suite of website tools for the Hanford Site (SOCRATES.pnnl.gov).

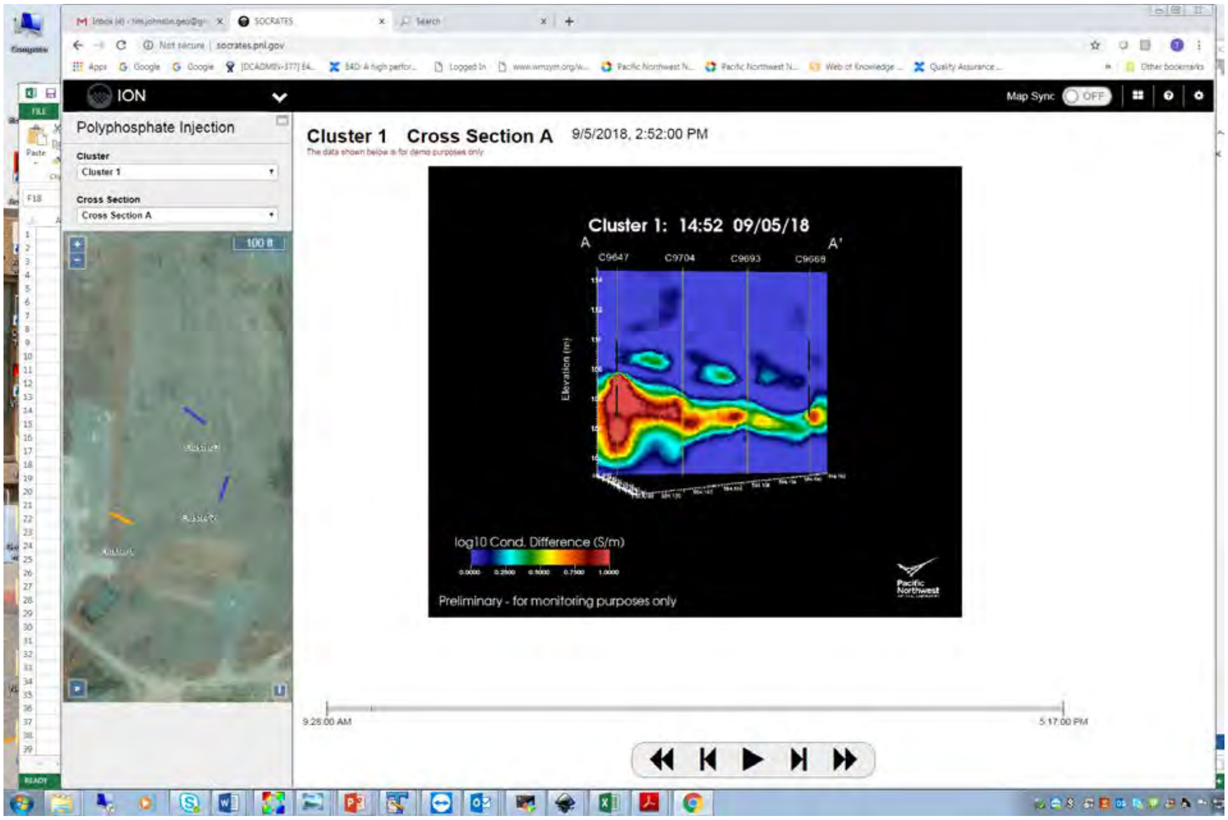

Figure 14. Example of the website used to monitor amendment distribution.

4.0 ERT Imaging Results

4.1 Pretreatment Baseline ERT Imaging

Baseline ERT image refers to the image of the bulk conductivity distribution prior to phosphate amendment injections in a given cluster. The baseline image is critical because it is subtracted from every time-lapse image to reveal the change in bulk conductivity with time. In this way, the change in bulk conductivity can be attributed to be caused by the increase in saturation and/or pore fluid conductivity due to the presence of phosphate amendment and/or carrier fluid (see Eq. 1.2). The baseline image can be used to also interpret geologic structure or other properties related to spatial variations in porosity, saturation, pore fluid conductivity, texture, and mineralogy (see Eq. 1.1).

Pretreatment baseline ERT images and corresponding interpretations are shown in Figure 15. Each image was collected on September 4, 2018, just prior to initiation of amendment injections in Zone 1. The upper row shows the estimated spatial variability in bulk conductivity for each cluster; the lower row shows the same images annotated with lines to aid interpretation of structural continuity. In each cluster, the increase in saturation across the water table boundary (approximately 105.0 m elevation) is clearly evident as an increase in bulk conductivity from above to below the water table. Each cluster also exhibits a relatively layered bulk conductivity structure from 105 m to approximately 110 m in elevation, with more massive structure above approximately 110 m in each case. In comparison to Clusters 2 and 3, Cluster 1 exhibits elevated conductivity, particularly above approximately 109 m elevation.

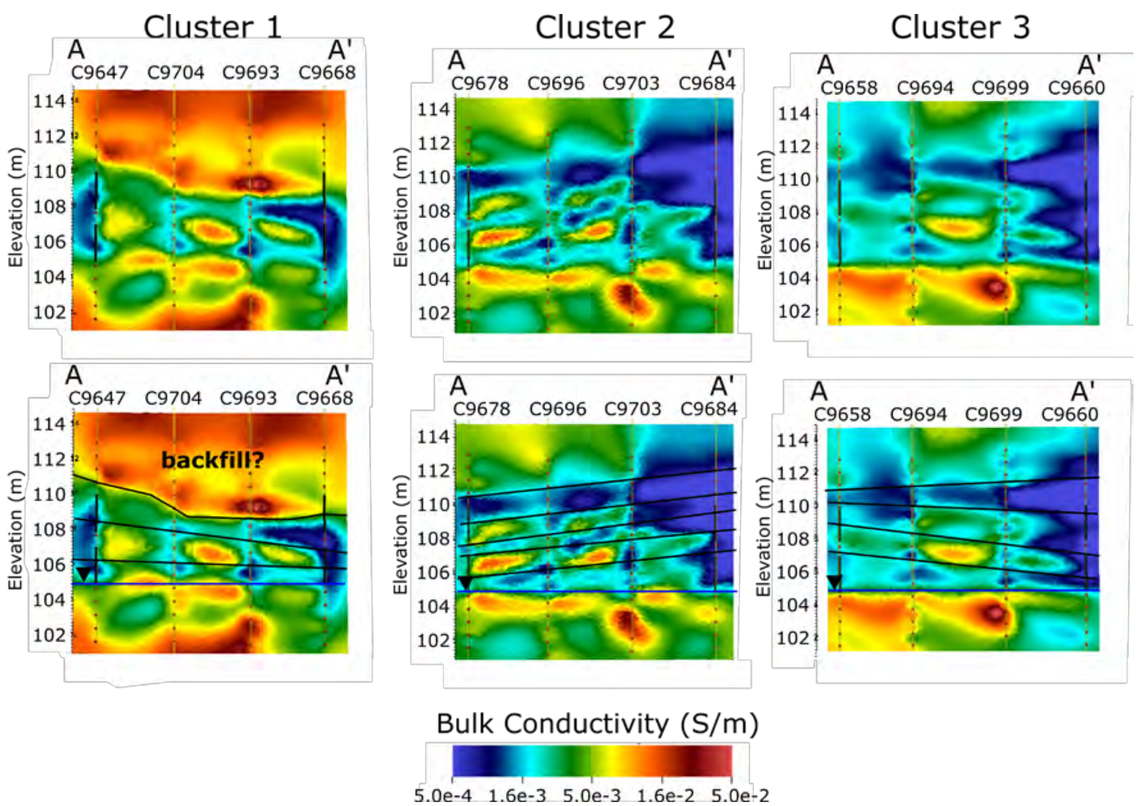

Figure 15. Pretreatment baseline ERT images in the A-A’ plane for each cluster (top) and the corresponding interpretations (bottom).

Cluster 1 is deployed directly beneath a historical waste discharge zone (BHI-01165, Rev 0). Previous remediation actions in the area of Cluster 1 included removal of contaminated near-surface materials and replacement with clean backfill. It is possible that the upper black line in the annotated (lower) Cluster 1 image is the excavation boundary and materials above that line consist of clean backfill with properties that promote relatively high bulk conductivity.

Eq. 1.1 provides insight into the possible mechanisms for the high and low bulk conductivity variations evident from the water table to the 110-112 m elevation in each cluster. In the vadose zone, finer grained materials generally tend to exhibit elevated matric potential in comparison to coarser grained sediments, and therefore exhibit elevated saturation levels, causing a corresponding increase in bulk conductivity. Consequently, regions of elevated bulk conductivity may be indicative of finer grained materials with higher baseline saturation levels than regions of depressed bulk conductivity. Furthermore, contaminated pore water generally exhibits elevated ionic strength and fluid conductivity in comparison to clean pore water. Contaminated pore water may contribute to regions of elevated bulk conductivity. Finally, historical discharge of contaminated water may have been accompanied by dissolution or precipitation reactions that altered both the physical structure and chemical composition of vadose zone sediments. For example, precipitation reactions could cause an increase in matric potential, saturation, and bulk conductivity. Precipitation of metallic minerals would be expected to cause an increase in the surface conductivity term ($\sigma_{s,t}$) of Eq. 1.1, thereby elevating bulk conductivity.

Although the baseline ERT images alone cannot uniquely determine which properties (porosity, saturation, fluid conductivity, or surface conductivity) are governing spatial variations in bulk conductivity, they provide important clues concerning the behavior of amendment transport and interpretation of the time-lapse ERT images. From A to A’, both Clusters 2 and 3 exhibit a transition from higher conductivity to low bulk conductivity near wells C9684 and C9660, respectively. Both of these wells are located within Injection Zone 3 and represent the eastern extent of ERT monitoring zones (Figure 6). As will be shown, the time-lapse ERT imaging suggests zones of elevated baseline bulk conductivity are relatively resistant to amendment infiltration in comparisons to zones of depressed baseline bulk conductivity. This provides further evidence that zones of elevated bulk conductivity may exhibit higher matric potentials and saturation levels (i.e., finer grained materials) in comparison to zones of relatively low bulk conductivity.

4.2 Observed vs. Simulated Data

ERT image quality and resolution is dependent in part on the level of random noise in field data, how accurately noise is specified in the inversion, and how well observed data are reproduced with respect to specified noise levels. Noise levels were estimated by collecting approximately 50 repeat pretreatment ERT surveys of 1,082 measurements on each cluster starting September 2, 2018, prior to amendment injections when subsurface conditions were assumed to be static. The 50 repeat measurements were then used to compute estimated standard deviations for each of the 1,313 measurements per cluster. Measurements with baseline coefficient of variation greater than 20% were removed from the baseline ERT survey and from each subsequent time-lapse survey. Standard deviations for each measurement were then used to specify the convergence criteria for the inversion. Figure 16 shows the data fit for the Cluster 1 baseline inversion, which is indicative of low noise data and corresponding ability to simulate those data with coherent ERT images. Low magnitude measurements generally exhibit smaller signal-to-noise ratios and are therefore not highly constrained by the inversion, which explains the relatively large deviations between observed and simulated low magnitude data. Similar convergence criteria were specified and achieved for each baseline and time-lapse inversion in each cluster, with slightly higher noise levels observed for Cluster 3.

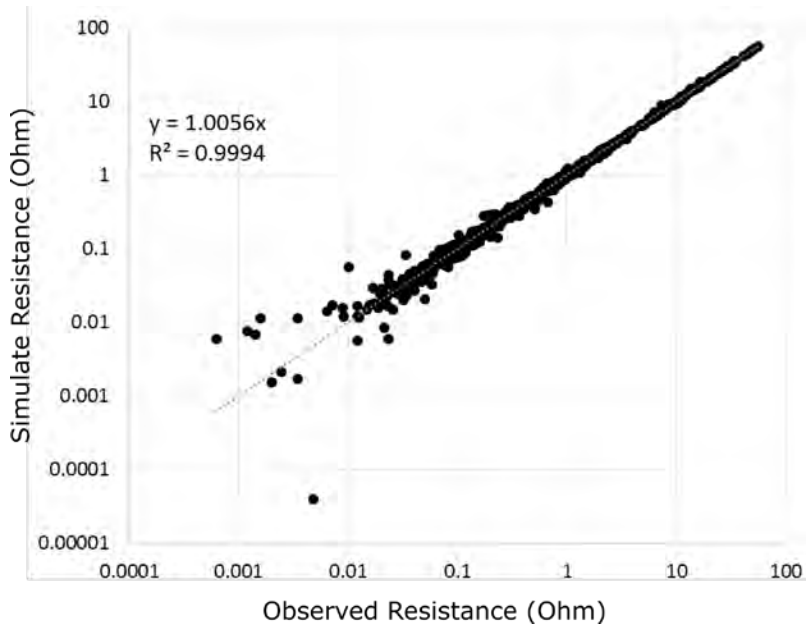

Figure 16. Nominal observed vs. simulated data fit at convergence.

4.3 Time Lapse ERT Images

Selected time-lapse imaging results for Clusters 1-3 are shown in Figure 17-Figure 19, respectively. Imaging results are shown twice daily for those days when amendment injections occurred on each cluster, once each morning just before injections began and once each afternoon just before injections ended. Morning pre-injection images show the amendment impacted regions due to injection operations prior to the current day. Afternoon images show the amendment impacted regions due to all injection operations including the current day.

4.3.1 Cluster 1 Imaging Results

Figure 17 shows the time-lapse imaging results for Cluster 1. Injections commenced on September 4, 2018, in the PRZ screen of well C9647. The September 4, 17:52 images suggest the amendment mounded over the top of the PRZ screen and flowed laterally in the vadose at least to monitoring well C9704. Increases in bulk conductivity to the A’ side, east of C9704, is likely due to amendment transport in the saturated zone at or near the water table, assumed to be at the 105.0 m elevation. The same images and all images for Cluster 1 show significant increases in bulk conductivity below the water table, particularly beneath injection wells, suggesting a significant fraction of the amendment exhibited density-driven downward flow in the saturated zone and pressure-driven radial flow at or near the water table.

In comparison to the September 4, 17:52 images, the September 5, 05:16 images show decreased change in bulk conductivity indicative of the draining and dilution of amendment after injection ended on September 4. Post-injection draining and dilution, and corresponding decrease in conductivity, occur in every morning image in every cluster. PRZ injections in C9647 repeated on September 5 and 6, with each successive day exhibiting an increase in the treated PRZ area between C9647 and C9704, in addition to increased amendment concentrations within the saturated zone apparently caused by both density-driven flow beneath the injection well and pressure-driven flow radially outward from the injection well.

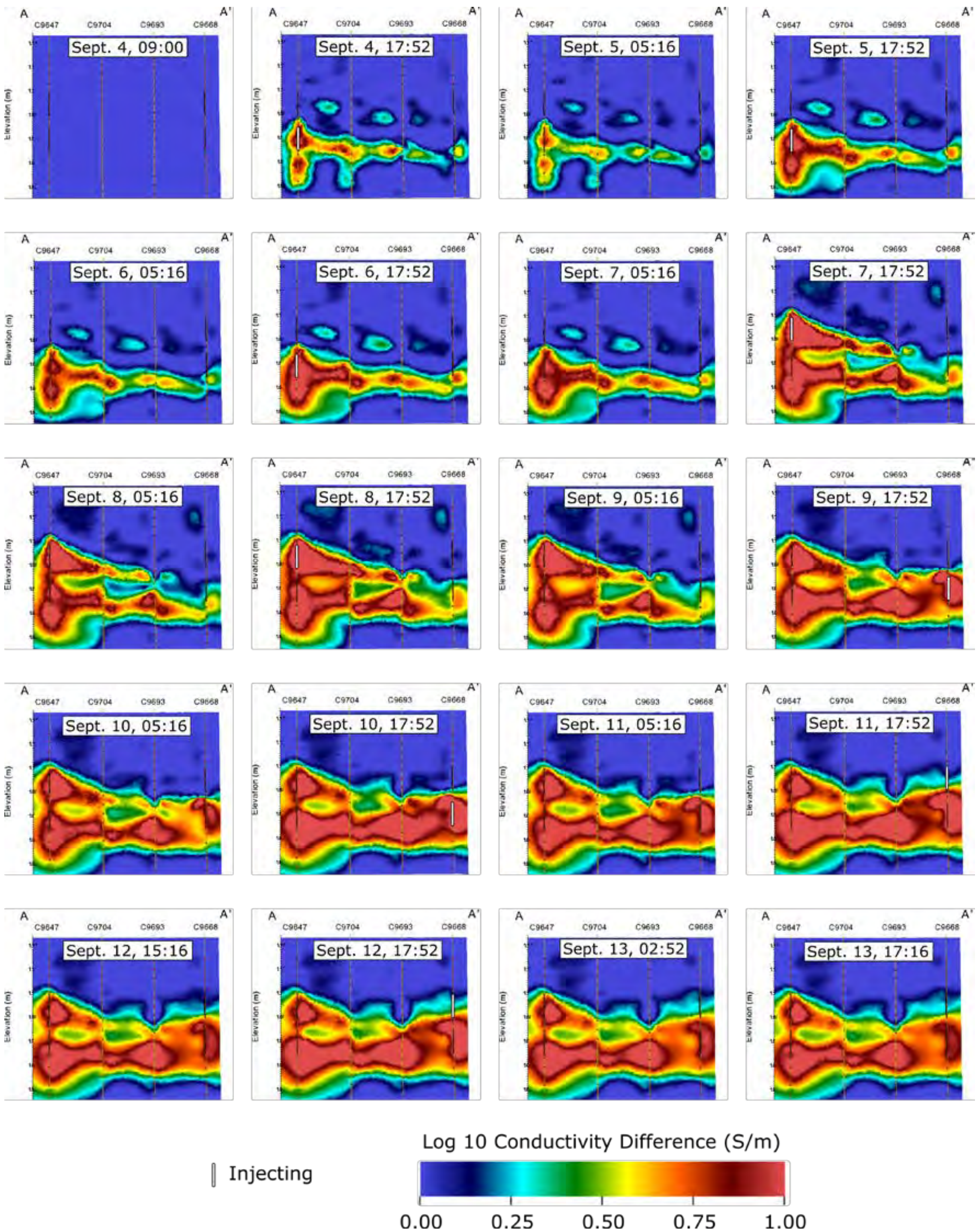

Figure 17. Twice-daily images of the ERT images that estimated amendment distribution in Cluster 1 during Zone 1 and 2 injections. Morning images are just prior to start of injection each day. Afternoon images are just prior to end of injection each day. Active injection well screen interval indicated.

Injection in the LVZ screen on C9647 commenced on September 7, 2018. As with the PRZ injection, amendment mounded over the top of the screened interval indicating that sediment permeability near C9647 was low enough to cause backpressure to build in the injection interval. Corresponding lateral amendment transport extended through C9704, past C9693, and appears to have reached injection well C9668 in the water table. In comparison to the PRZ injection, increases in saturated zone bulk conductivity were evident but marginal, suggesting that much of the amendment was distributed within the vadose zone. LVZ injection in C9647 on September 8 appears to have impacted the same region as the September 7 LVZ injection, but elevated bulk conductivity in comparison to September 7 suggests higher overall amendment concentrations within the zone of amendment distribution after the September 8 injections.

Injection in the PRZ screen of C9668 commenced on September 9. Significant mounding over the top of the PRZ screened interval was evident (see September 9, 17:52 image). Lateral transport extended the amendment-distribution zone to approximately 108 m in elevation between C9668 and C9693, and appears to have increased amendment concentrations in the vadose between C9693 and C9704, which was also impacted by the C9647 injections. PRZ injection on C9668 repeated on September 10. That injection did not extend but did increase amendment concentration within the previous region of amendment distribution.

LVZ injection in C9668 commenced on September 11 (see September 11, 17:52 image). In this case, amendment levels did not rise to the top of the screened interval, suggesting sediment permeability was high enough to inhibit backpressure and amendment mounding. Consequently, lateral transport did not appear to be as extensive as the C9647 LVZ injection. However, amendment concentrations do appear to have increase in the vadose zone between C9704 and C9693 as a result of the C9668 LVZ injection (compare September 10, 17:52 and September 11, 17:52 images). LVZ injection on C9668 repeated on September 12, 2018, but did not appear to significantly increase the amendment-distribution zone extent or concentrations compared to the September 11 injection (compare September 11, 17:52 and September 12, 17:52 images).

Overall, the ERT images suggest amendment injections in Cluster 1 exhibited significant lateral transport, impacting all of the PRZ and much of the LVZ.

4.3.2 Cluster 2 Imaging Results

ERT imaging results for Cluster 2 are shown Figure 18. Injection into PRZ screen of wellbore C9678 commenced on September 9, 2018, and was repeated on September 10. The September 9, 17:02 image suggests that the amendment may have reached the top of the screened interval, but likely did not mound above the screen. Lateral transport of amendment appeared to extend past wellbore C9696, but did not appear to reach C9703 within the vadose zone. As observed in Cluster 1, amendment transport within the saturated zone appears to have been dominated by density-driven flow near the wellbores, with pressure-driven radial flow primarily near the water table, extending away from the injection well. The repeat injection on September 10 appears to have extended the amendment-distribution zone slightly in both the vertical and lateral directions, and deeper within the saturated zone.

Injection into the LVZ screen of wellbore C9678 commenced on September 11. Amendment did not appear to reach the top or mound above the screened interval (see September 11, 17:03 images). Laterally, the amendment-distribution zone appeared to extend nearly to but not past wellbore C9696 within the vadose zone. Amendment transport from this screen appears to have resulted in a relative dome-shaped amendment-distribution zone lying atop the amendment from the PRZ injection in the same well.

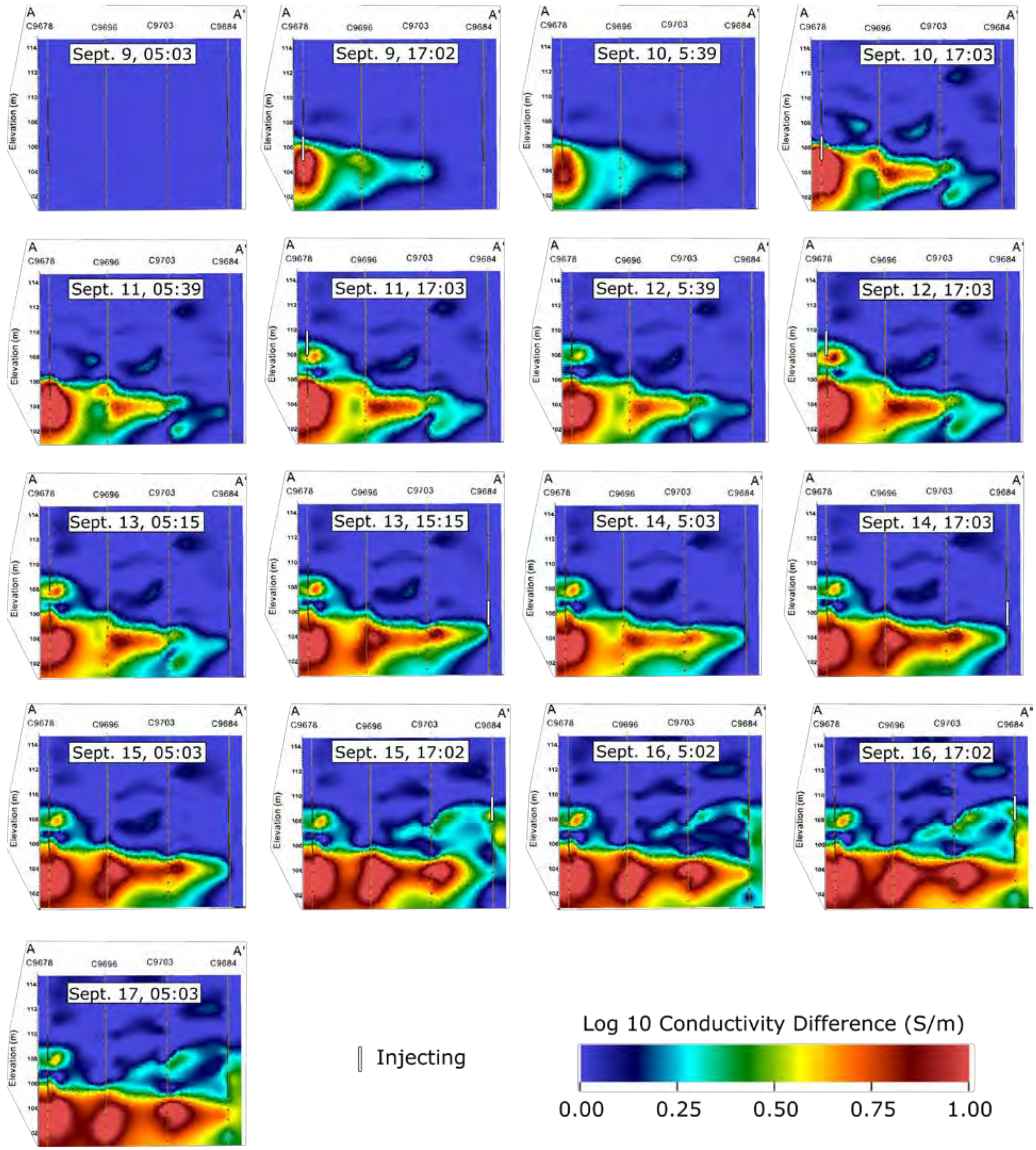

Figure 18. Twice-daily images of the ERT estimated amendment-impacted zone in Cluster 2 during Zones 2 and 3 injections. Morning images are just prior to start of injection each day. Afternoon images are just prior to end of injection each day. Active injection well screen interval indicated.

There also appeared to be a low-permeability lens between the PRZ and LVZ screens that received amendment. Repeat injection on September 12 did not appear to extend the amendment-distribution zone, but did appear to increase amendment concentration within this zone.

Injection into the PRZ screen of wellbore C9684 commenced on September 13. Amendment from this injection appeared to have transported nearly directly to the saturated zone with minimal distribution to the vadose zone. There was no indication of any significant mounding within the screened interval or subsequent transport of amendment through the vadose zone. Repeat injection on September 14 did not appear to extend the amendment-distribution zone within the vadose zone, but did appear to increase amendment concentrations within the saturated zone (compare September 13, 15:15 and September 14, 17:03 images).

Injection into the LVZ screen of wellbore C9684 commenced on September 15. Amendment mounding near the wellbore did not appear to have extended to the top of the wellbore screen. Lateral transport appeared to have reached past wellbore C9703 to approximately midway between wellbores C9703 and C9696 within the vadose zone. Repeat injection on September 16 appeared to have slightly extended the horizontal and vertical extent, and increased the amount of amendment within the amendment-distribution zone. There also appeared to be a low permeability lens within the overall C9684 LVZ amendment-distribution zone that was not infiltrated with amendment in either the initial or repeat injection.

4.3.3 Cluster 3 Imaging Results

ERT imaging results for Cluster 3 are shown in Figure 19. Re-analysis of the real-time imaging data revealed several ERT measurements with degrading quality over the course of the monitoring period. To produce consistent imaging results over time, those measurements were removed from the analysis. Most of the culled measurements were associated with injection wells C9658 and C9660. This resulted in decreased resolution near those wells in comparison to Clusters 1 and 2, particularly near the PRZ screen in C9660. Resolution near wellbores C9694 and C9699 were not significantly influenced. Interpretation of the ERT imaging results for Cluster 3 are presented in this context below.

Injection into the PRZ screen of C9660 commenced on September 13. Reduced resolution near C9660 near the PRZ resulted in no response near C9660, and therefore no interpretation could be made concerning amendment distribution in the vadose zone near that well (see September 13, 17:27 images). Increases in bulk conductivity were evident near the water table at C9699, C9694, and C9658, suggesting lateral pressure-driven transport near the water table, similar to that observed in Clusters 2 and 3. There was no indication that amendment reached wellbore C9699 within the vadose zone. Repeat injection on September 14 appears to have increased the amount of amendment within the previous amendment-distribution zone, but did not indicate an extension of this zone near C9699.

Injection into the LVZ screen of C9660 commenced on September 15 (see September 15, 17:26 images). Amendment mounding did not appear to reach the top of the LVZ screened interval. Lateral transport appeared to have nearly reached C9699 through a relatively transmissive zone at approximately 108 m elevation. Repeat injection on September 16 appeared to have increased the amount of amendment in the saturated zone, but did not appear to increase the extent of amendment in the vadose zone. In the days following September 17, bulk conductivity values appeared to have returned to baseline conditions, which may indicate relatively rapid draining of amendment toward the water table after injection. Well C9660 exhibited relatively low vadose zone bulk conductivity, which may be indicative of coarser grained materials that are not conducive to horizontal flow under the induced injection conditions. Amendment migration from C9660 appeared to have been dominated by vertical transport, particular from the PRZ injection interval.

Injection into the PRZ screen of well C9658 commenced on September 17. Amendment mounding does not appear to have reached the top of the screen and impact above the water table appeared to have been minimal for this injection. Repeat injection on September 18 exhibited enhanced mounding near the screen as well as enhanced lateral extension of amendment above the water table. The amendment-distribution zone did not appear to have reached wellbore C9694 in the vadose zone as a result of either the initial or repeat injection in the C9658 PRZ screen.

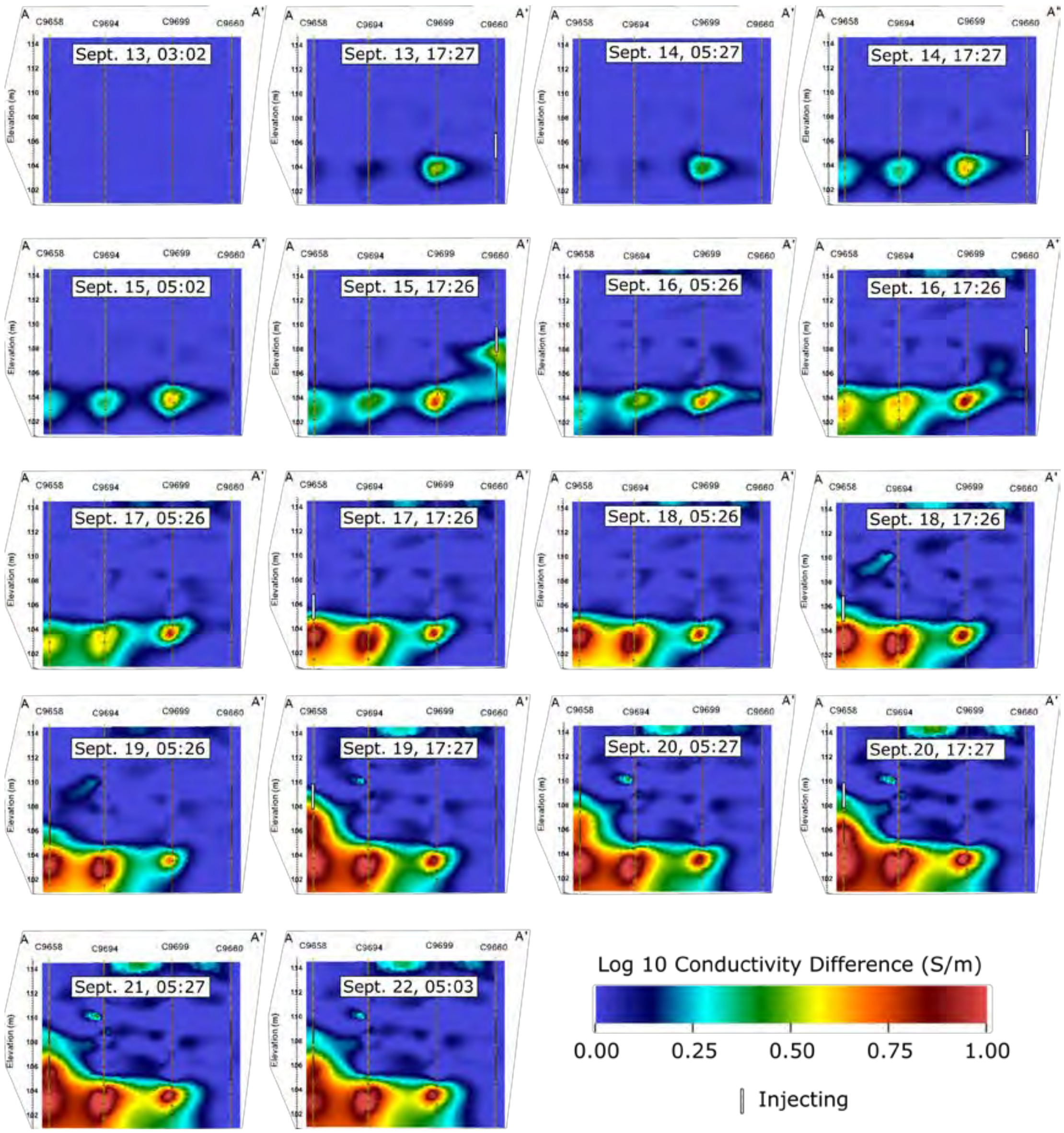

Figure 19. Twice-daily images of the ERT estimated amendment-impacted zone in Cluster 3 during Zones 3 and 4 injections. Morning images are just prior to start of injection each day. Afternoon images are just prior to end of injection each day. Active injection well screen interval indicated.

Injection into the C9658 LVZ screened interval commenced on September 19. Amendment mounding appeared to reach approximately half-way up the LVZ screen. Lateral transport appeared to have approached, but did not reach wellbore C9694. Repeat injection on September 20 appeared to have slightly enhanced lateral transport and increased the amount of amendment in the vadose zone and groundwater in comparison to the initial injection (compare September 19, 17:27 and September 20, 17:27 images). Overall injection into the C9658 LVZ screen appeared to have resulted in a relatively dome-shaped amendment-distribution zone that terminated at the water table before reaching wellbore C9694.

5.0 Imaging Result Interpretation

Figure 20 shows the maximum increase in bulk conductivity exhibited during injection operations in each of the clusters, or equivalently the ERT estimated amendment-distribution zone. These images were produced by extracting the maximum change in bulk conductivity exhibited over the entire monitoring period at each imaging pixel and plotting the resultant images as shown in Figure 20. Amendment transport in Cluster 1 exhibited significant vertical and lateral flow in comparison to Clusters 2 and 3, resulting in widespread coverage of LVZ and PRZ sediment between injection wells. Cluster 2 exhibited enough lateral flow to reach the LVZ and PRZ near the injection wells, but only the PRZ appeared to have been reached by amendment in the region between injection wells. Cluster 3 exhibited the smallest amount of lateral flow and appeared to have been reached by amendment primarily near the injection wells. Imaging results below the water table suggest that the zone of amendment distribution penetrated deeper into the saturated zone in Clusters 2 and 3 than in Cluster 1.

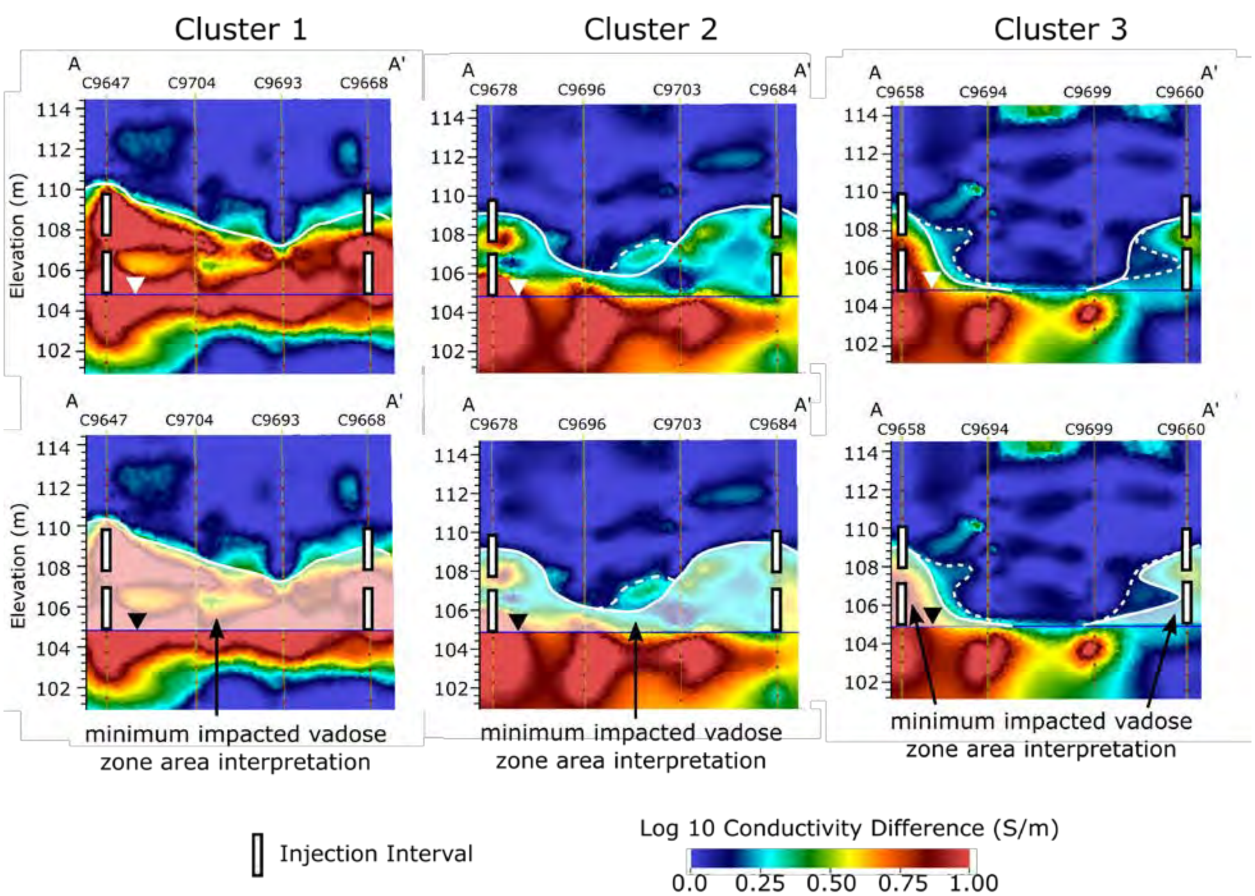

Figure 20. Maximum change in conductivity observed for each cluster. Solid lines are interpretations of the amendment-distribution zone boundary. Dotted lines are alternate interpretations.

Lateral transport within the three clusters is correlated with differences in LVZ and PRZ sediments that are evident in baseline static ERT imaging. Close inspection of the final amendment-distribution zones in comparison to the baseline images show that apparent gaps in amendment coverage within the vadose zone are generally associated with zones of elevated conductivity in the baseline images. This is consistent with the interpretation that elevated regions of baseline conductivity represent finer grained units with lower permeability, elevated saturation, and possibly elevated pore fluid conductivity resulting from past waste-discharge operations. This is also consistent with the time-lapse imaging results. Namely, the extensive lateral transport observed in Cluster 1 is consistent with horizontally continuous layers of fine-grained sediments interbedded with coarser grained sediments. The finer grained interbeds act as vertical flow barriers and encourage lateral flow through the coarser grained bedding. Conversely, lower bulk conductivity zones in Clusters 2 and 3 correspond to regions of limited lateral amendment transport, or enhanced, gravity-driven vertical transport through relatively permeable sediments.

6.0 References

BHI-01164 Rev 0. 1998. *300 Area Process Trenches Verification Package*. Bechtel Hanford, Inc., Richland, Washington.

DOE/RL-2005-41. 2005. *Work Plan for Phase III Feasibility Study 300-FF-5 Operable Unit*. U.S. Department of Energy, Richland Operations Office, Richland, Washington.

DOE/RL-2017-66 Rev 0. 2018. *Hanford Site Groundwater Monitoring Report for 2017*. U.S. Department of Energy, Richland Operations Office, Richland, Washington.

DOE/RL-2014-42-ADD1. 2016. *300-FF-5 Operable Unit Remedy Implementation Sampling and Analysis Plan Addendum for Stage B Uranium Sequestration*. U.S. Department of Energy, Richland Operations Office, Richland, Washington.

EPA and DOE. 2013. *Hanford Site 300 Area Record of Decision for 300-FF-2 and 300-FF-5, and Record of Decision Amendment for 300-FF-1*. U.S. Environmental Protection Agency and U.S. Department of Energy, Richland, Washington.

Johnson TC, RJ Versteeg, A Ward, FD Day-Lewis, and A Revil. 2010. “Improved hydrogeophysical characterization and monitoring through parallel modeling and inversion of time-domain resistivity and induced-polarization data.” *Geophysics* 75(4): Wa27-Wa41.

Peterson RE, ML Rockhold, RJ Serne, PD Thorne, and MD Williams. 2008. *Uranium Contamination in the Subsurface Beneath the 300 Area, Hanford Site, Washington*. PNNL-17034, Pacific Northwest National Laboratory, Richland, Washington.

SGW-60778 Rev 0. 2019. *300-FF-5 Operable Unit Stage B Uranium Sequestration System Installation Report*. CH2M HILL Plateau Remediation Company, Richland, Washington.

Slater LD and D Lesmes. 2002. “IP interpretation in environmental investigations.” *Geophysics* 67(1):77-88.

Szecsody JE, L Zhong, M Oostrom, VR Vermeul, JS Fruchter, and MD Williams. 2012. Use of Polyphosphate to Decrease Uranium Leaching in Hanford 300 Area Smear Zone Sediment. PNNL-21733, Pacific Northwest National Laboratory, Richland, Washington.

Williams BA, CF Brown, W Um, MJ Nimmons, RE Peterson, BN Bjornstad, and DC Lanigan. 2007. Limited Field Investigation Report for Uranium Contamination in the 300 Area, 300-FF-5 Operable Unit, Hanford Site, Washington. PNNL-16435, Pacific Northwest National Laboratory, Richland, Washington.

Appendix A – Raw Data and E4D-Formatted Files

All of the raw electrical resistivity tomography (ERT) data files are provided in digital format with this report. In addition, all of the E4D input files are provided to enable reproducibility of the imaging results. ERT time-lapse difference images are also included. Users should refer to Multiphase Technologies, LLC., documentation for the MPT-DAS 1 electrical impedance tomography system for details concerning the format of the raw ERT data files (although they are somewhat self-explanatory). E4D file formats are described in detail in the E4D User Guide, which is downloadable at https://e4d.pnnl.gov. The files provided are described in Table A.1.

Table A.1. Bulk conductivity time-series data file formats.

File Name	Content	Format
clus*.1.node	E4D node file for cluster *	Tetgen node file
clus*.1.ele	E4D element file for cluster *	Tetgen element file
clus*.1.face	E4D face file for cluster *	Tetgen face file
clus*.1.neigh	E4D neighbor file for cluster *	Tetgen neighbor file
clus*.1.edge	E4D edge file for cluster *	Tetgen edge file
clus*.trn	E4D trans file for cluster *	E4D mesh translation file
clus*_base.inv	E4D baseline inversion options	E4D inversion options file
clus*_tl.inv	E4D time-lapse inversion options	E4D inversion options file
clus*.out	E4D output options	E4D output options file
CLS*DPS2_YYYYMMDD_HHmm.sig	E4D inversion for cluster* at year HHHH, month MM, day DD, hour HH, and minute mm.	E4D conductivity file
CLS*DPS2_YYYYMMDD_HHmm.sig	ERT survey data for cluster* at year HHHH, month MM, day DD, hour HH, and minute mm.	MPT-DAS1 TDIP file
CLS*DPS2_YYYYMMDD_HHmm.png	ERT time-lapse difference image for cluster* at year HHHH, month MM, day DD, hour HH, and minute mm.	Portable Network Graphic (PNG) file

PNNL-28619

Pacific Northwest National Laboratory

902 Battelle Boulevard
P.O. Box 999
Richland, WA 99354
1-888-375-PNNL (7665)

www.pnnl.gov